THE JOURNAL OF BIOLOGICAL CHEMISTRY VOL. 286, NO. 50, pp. 43324–43333, December 16, 2011

Identification of an Endocytosis Motif in an Intracellular Loop of Wntless Protein, Essential for Its Recycling and the Control of Wnt Protein Signaling*

Received for publication, September 27, 2011, and in revised form, October 21, 2011 Published, JBC Papers in Press, October 25, 2011, DOI 10.1074/jbc.M111.307231

Isabelle Gasnereau[‡1], Patrick Herr[§1], Pei Zhi Cheryl Chia[‡1,2], Konrad Basler[§], and Paul A. Gleeson[‡3]

From the [‡]Department of Biochemistry and Molecular Biology and Bio21 Molecular Science and Biotechnology Institute, The University of Melbourne, Victoria 3010, Australia and the [§]Institute of Molecular Life Sciences, University of Zürich, Winterthurerstrasse 190, CH-8057 Zürich, Switzerland

Background: The secretion of Wnt molecules is dependent on the multipass membrane-sorting receptor, Wntless.
Results: A tyrosine-based internalization motif has been identified in an intracellular loop of Wntless.
Conclusion: Endocytosis of Wntless is required for efficient secretion of Wnt signaling molecules.
Significance: Defining the sorting signals and intracellular trafficking of Wntless is crucial to appreciate the regulation of Wnt secretion and development processes.

The secretion of Wnt signaling proteins is dependent upon the transmembrane sorting receptor, Wntless (Wls), which recycles between the *trans*-Golgi network and the cell surface. Loss of Wls results in impairment of Wnt secretion and defects in development and homeostasis in *Drosophila*, *Caenorhabditis elegans*, and the mouse. The sorting signals for the internalization and trafficking of Wls have not been defined. Here, we demonstrate that Wls internalization requires clathrin and dynamin I, components of the clathrin-mediated endocytosis pathway. Moreover, we have identified a conserved *YXXϕ* endocytosis motif in the third intracellular loop of the multipass membrane protein Wls. Mutation of the tyrosine-based motif YEGL to AEGL (Y425A) resulted in the accumulation of human mutant Wls on the cell surface of transfected HeLa cells. The cell surface accumulation of Wls^{AEGL} was rescued by the insertion of a classical *YXXϕ* motif in the cytoplasmic tail. Significantly, a *Drosophila* Wls^{AEGL} mutant displayed a wing notch phenotype, with reduced Wnt secretion and signaling. These findings demonstrate that *YXXϕ* endocytosis motifs can occur in the intracellular loops of multipass membrane proteins and, moreover, provide direct evidence that the trafficking of Wls is required for efficient secretion of Wnt signaling proteins.

The Wnt family of signaling molecules regulate a plethora of developmental processes in animals (1). The secretion of Wnt molecules has been shown to be dependent upon the transmembrane sorting receptor, Wntless (Wls[4]; also know as Evenness interrupted and Sprinter in *Drosophila* and MOM-3/MIG-14 in *Caenorhabditis elegans*) (2–4). Wls is specific cargo receptor for delivery of Wnts from the *trans*-Golgi network (TGN) to the cell surface (5). The function of Wls is highly conserved in evolution and has been shown to regulate Wnt secretion in a number of species including *C. elegans*, *Drosophila*, mice, and human (2, 3, 6–8). Loss of Wls results in an impairment of Wnt secretion and defects in development and homeostasis in *Drosophila*, *C. elegans*, and mice.

Wls recycles between the TGN and the cell surface via endosomes (9–12). The recycling of Wls by retrograde transport from endosomes to the TGN allows Wls to be used multiple times in assisting the anterograde transport of newly synthesized Wnt molecules from the Golgi to the cell surface. Perturbation of clathrin-mediated endocytosis or endosomal sorting results in a block in recycling of Wls and reduction in Wnt secretion (9–14), highlighting the importance of the recycling of Wls for efficient Wnt secretion. The endosome-to-TGN transport of Wls in *Drosophila*, *C. elegans*, and humans cells is dependent on the retromer complex (9–14), implying that a similar retrograde transport pathway is used by Wls in different organisms.

The internalization and intracellular trafficking of membrane proteins require specific signals. Wls is a multipass membrane protein that spans the membrane seven or eight times, depending on whether the signal sequence is cleaved (15, 16). However, the signals/motifs for internalization and endosomal sorting of Wls have not been identified. To date, the importance of Wls recycling has been examined by the silencing and knockout of components of trafficking machinery, approaches that are likely to influence the transport of a range of other cargos. Identification of the trafficking motifs of Wls would allow the generation of Wls mutants that are blocked in recycling. In this paper we have identified a functionally active *YXXϕ* motif in the third intracellular loop of Wls and demonstrate that this motif is required for its internalization in human cells and *Drosophila*. Moreover, we present data that demonstrate that the internalization-defective Wls mutant in *Drosophila* results in reduced Wnt secretion.

* This work was supported by the National Health and Medical Research Council of Australia and the Swiss National Science Foundation.
[1] These authors contributed equally to this work.
[2] Supported by a Melbourne International Graduate scholarship.
[3] To whom correspondence should be addressed. Tel.: 61-3-8344-2354; Fax: 61-3-9348-1428; E-mail: pgleeson@unimelb.edu.au.
[4] The abbreviations used are: Wls, Wntless; CHC17, heavy chain isoform of clathrin; DAPI, 4′,6-diamidino-2-phenylindole dihydrochloride; Sens, Senseless; TGN, *trans*-Golgi network; Tx Red-ConA, Texas Red-conjugated concanavalin A; Wg, Wingless.

EXPERIMENTAL PROCEDURES

Plasmids, Antibodies, Reagents, and siRNA—pcDNA3-hWls^{wt}-HA has been described (2) and encodes the human Wls protein (ABD58927.1) with a HA epitope on the C terminus. pcDNA3-hWls^{AEGL}-HA, encoding the protein hWls^{AEGL} (Y425A), was obtained using the primers 5′-CAAAGTCCCGCGGCTACACGCCGAGGGGCTAATTTTTAGGTTCAAGTTCC-3′ and 3′-GGAACTTGAACCTAAAAATTAGCCCCTCGGCGTGTAGCCGCGGGACTTTG-5′. The pcDNA3-hWLS-AEGL/PYQRL-HA (hWls$^{A/PYQRL}$-HA) construct was obtained using the primers 5′-TATGCACCATCCCATAAACCCTATCAAAGACTCCAGTCCAATGGCGATCTG-3′ and 5′-CAGATCGCCATTGGACTGGAGTCTTTGATAGGGTTTATGGGATGGTGCATA-3′ by site-directed mutagenesis using the pcDNA3-hWls^{AEGL}-HA construct as template.

Wild-type (wt) and dominant negative (K44A) dynamin I in the pCB1 mammalian expression vector were a kind gift from Sandra Schmidt (Scripps Institute) (17). Rabbit antibodies to *Drosophila* Wls have been described (11), and rabbit antibodies to the HA tag were from Cell Signaling Technology. Guinea pig polyclonal antibodies to Senseless (Sens) were a gift from H. Bellen (Baylor College of Medicine, Houston, TX) (18). Monoclonal antibodies to human golgin-97 and rat clathrin heavy chain were from BD Biosciences, and Wingless (Wg) was from the Developmental Studies Hybridoma Bank (clone 4D4). Goat polyclonal antibodies to dynamin I (C-16) were from Santa Cruz Biotechnology. Secondary antibodies for immunofluorescence were goat anti-rabbit IgG-Alexa Fluor 488, goat anti-mouse IgG-Alexa Fluor 568, goat anti-mouse IgG-Alexa Fluor 594, goat anti-guinea pig IgG-Alexa Fluor 568, and donkey anti-goat IgG-Alexa Fluor 647 purchased from Molecular Probes. The siRNA to the heavy chain isoform of clathrin (CHC17) has been described previously (19) and was purchased from Sigma Proligos (Lismore, Australia).

Cell Culture and Transient Transfections—HeLa cells were maintained as semiconfluent monolayers in Dulbecco's modified Eagle's medium (DMEM) supplemented with 10% (v/v) fetal calf serum (FCS), 2 mM L-glutamine, 100 units/μl penicillin, and 0.1% (w/v) streptomycin (C-DMEM) in a humidified 10% CO_2 atmosphere at 37 °C. For DNA transient transfections, HeLa cells were seeded as monolayers and transfected using FuGENE 6 (Roche Diagnostics) according to the manufacturer's instructions. Transfections were carried out in C-DMEM at 37 °C, 10% CO_2 for 24 h.

siRNA Transfections—Transient transfections with siRNA were performed using Oligofectamine (Invitrogen) according to the manufacturer's instructions, for 72 h prior to analysis. CHC17 was silenced in HeLa cells with a human CHC17 siRNA target sequence (19).

Immunoblotting—Cell extracts were dissolved in reducing sample buffer, and samples were resolved on a 4–12% NuPAGE precast gradient gel. Immunoblotting was performed as described (Lieu *et al.*, 2007). Analysis of images was performed using the Gel Pro Analyzer program (MediaCybernetics, Bethesda, MD)

Drosophila Mutants and Rescue Experiments—The 5519-bp genomic region of *wls*^{1} was cloned using endogenous restriction sites EcoRI/NotI into a pattB vector. The Wls^{wt} and Wls^{AEGL} (Y435A) constructs were introduced to the landing site WD-51D on the second chromosome. The transgenes were combined with the *wls*^{1} allele on the third chromosome. Rescue efficiency was assessed by loss of the balancer chromosome. For Wls^{wt} 681 animals were counted and 667 for Wls^{AEGL}. According to Mendelian ratios the rescue efficiency was 60% for Wls^{wt} and 50% for Wls^{AEGL}.

Indirect Immunofluorescence, Image Analysis—Mammalian cells on coverslips were fixed with 4% paraformaldehyde for 15 min or methanol (−20 °C) for 4 min, followed by quenching in 50 mM NH_4Cl/PBS for 10 min. Cells were permeabilized in 0.1% Triton X-100/PBS for 4 min and incubated in 5% FCS/PBS for 20 min to reduce nonspecific binding. Monolayers were incubated with primary and secondary conjugates as described. Nuclei were stained with 4′,6-diamidino-2-phenylindole dihydrochloride (DAPI) (Sigma-Aldrich) diluted to 1 μg/ml for 10 min, washed with PBS, then rinsed briefly in water. Coverslips were then blotted dry and mounted in Mowiol on a microscope slide. All images were acquired using a confocal laser scanning microsope (Leica LCS SP2 confocal imaging system) using a 100×/1.4 NA HCX PL APO CS oil immersion objective. Three-dimensional reconstructions were generated using the process option of the Leica LCS software. For multicolor labeling, images were collected independently.

Adult wings were dehydrated and mounted in Euparal Mountant (Taab Laboratories). Images were taken with a Zeiss Axioplan 2 microscope using Plan-Neofluar 5× and 20× objectives.

Wing imaginal discs were dissected and stained following standard protocols. Images were taken using the Zeiss LSM 710 with 20× and 63× oil objectives.

Isolation of Plasma Membrane Lawns—Plasma membrane lawns were prepared by a one-step procedure as described (20, 21). Coverslips were coated in poly-L-lysine (0.01% w/v) by immersion and dried before seeding with HeLa cells. Cultured cells were transfected with hWls constructs for 24 h as described above. Monolayers were rinsed three times in swelling buffer (0.7 mM magnesium acetate, 37 mM potassium acetate, 1.7 mM sodium acetate, 20 mM Hepes, 1 mM EGTA, pH 7.3) and then disrupted by ultrasonication (Sonics Vibracell) for 5 s at a power setting of 12 in 1 ml of PBS/well. Sonicated cells were immediately washed in PBS and fixed with 4% formaldehyde, quenched with 50 mM NH_4Cl/PBS, and blocked with 5% FCS/PBS prior to staining with Texas Red-conjugated concanavalin A (Tx Red-ConA) to detect membranes retained on coverslips, and anti-HA antibodies to detect cell surface expression of hWls protein. All images were scaled identically for fluorescence analysis of the isolated plasma membrane lawns.

Quantification of Immunofluorescence—Quantification of immunofluorescent cell images was carried out using the ImageJ program (National Institutes of Health public domain software) for 20–25 cells/dataset. Data are presented as the number of HA pixels at the Golgi region (outlined by staining with Golgi markers) relative to the total number of HA pixels/cell and are expressed as the mean ± S.E. and analyzed by an unpaired, two-tailed Student's *t* test.

For plasma membrane lawns, the total number of Tx Red-ConA pixels/frame (>20 frames/sample) was quantitated using the ImageJ program (National Institutes of Health public domain software) and used as a measure of the total membrane on coverslips. The number of HA pixels/frame was quantitated as a measure of cell surface hWls. Data are presented as the number of HA pixels/10^4 Tx Red-ConA pixels and are expressed as the mean ± S.E. and analyzed by an unpaired, two-tailed Student's *t* test.

A p value of <0.05 (*) was considered as significant, $p < 0.01$(**) was highly significant, and $p < 0.001$ (***) was very highly significant. The absence of a p value indicates that the differences were not significant.

RESULTS

Internalization of Wls Is Dependent on Clathrin-mediated Endocytosis—The recycling of Wls between the Golgi and plasma membrane is dependent on the internalization by endocytosis. There is considerable indirect evidence that Wls is internalized by clathrin-mediated endocytosis (10–13). For example, the secretion of Wnt proteins is reduced after silencing of AP2, suggesting that the recycling of Wls was affected by a block in this pathway (10, 11). Initially we carried out experiments to determine directly whether the multipass membrane Wls protein was internalized by the classical clathrin pathway. HeLa cells transfected with HA-tagged hWls (hWls^{wt}-HA) show a perinuclear localization that overlaps with the TGN marker golgin-97 at steady state (Fig. 1*A*). To assess the impact of clathrin depletion on Wls distribution, the ubiquitous CHC17 was silenced in HeLa cells with a previously characterized human CHC17 siRNA target sequence (19), followed by transfection with hWls^{wt}-HA. Immunofluorescence showed that the level of clathrin heavy chain was significantly reduced in CHC17 siRNA-transfected cells (Fig. 1*B*). From the analysis of both low and high expressing hWls^{wt}-HA cells (>100) the depletion of clathrin heavy chain dramatically altered the steady-state distribution of hWls. From optical sections and three-dimensional reconstructions of CHC17-depleted cells (Fig. 1, *B* and *Bi*), hWls^{wt}-HA was located predominantly at the cell surface, whereas in control siRNA-treated cells hWls^{wt}-HA was located predominantly in the Golgi, with only low levels detected at the cell surface (Fig. 1, *A* and *B*). We assessed the intracellular distribution by quantifying the proportion of Wls located in the Golgi region compared with the whole cell (percentage of total HA pixels in Golgi region). In control cells the majority (60%) of hWls^{wt}-HA was located within the Golgi; CHC17 depletion resulted in a 3-fold decrease in Golgi-localized Wls compared with untreated cells (Fig. 1*C*), consistent with the increased proportion of Wls at the cell surface.

Next, we directly quantified the level of Wls at the cell surface. As extensive attempts to generate an exofacially tagged Wls molecule all resulted in endoplasmic reticulum retention of the modified Wls, or inaccessible epitopes for antibody binding, we used an alternative approach and determined the level of Wls in plasma membrane lawns (20, 21). Plasma membrane lawns were isolated from either untransfected cells or cells transfected with hWls^{wt}-HA, and the level of hWls^{wt}-HA associated with the plasma membranes was determined by detection of the cytoplasmically oriented HA tag. Tx Red-ConA was used as a membrane marker and DAPI staining used distinguish between intact and disrupted cells. Whereas non-sonicated, intact cells showed extensive Tx Red-ConA staining of different membrane structures, nuclei-free, sonicated samples showed Tx Red-ConA-staining of membrane lawns attached to the coverslips (Fig. 2*A*), confirming the retention of plasma membranes on the coverslip. Whereas only low levels of hWls^{wt}-HA were detected associated with the plasma membrane lawns of control siRNA-treated cells, abundant hWls^{wt}-HA staining was associated with lawns derived from CHC17-depleted cells (Fig. 2, *B* and *C*). The level of hWls^{wt}-HA staining was normalized to the surface area of plasma membranes, as measured by Tx Red-ConA staining and the total cellular levels of hWls^{wt}-HA, as determined by blotting (Fig. 2*B*). Significantly, CHC17 siRNA treatment resulted in a 31-fold higher level of hWls^{wt}-HA associated with the plasma membrane lawns compared with control siRNA cells (Fig. 2*D*). These data confirm the accumulation of hWls^{wt}-HA on the cell surface of CHC17-depleted cells.

The distribution of hWls^{wt}-HA was also examined in cells expressing the dominant negative mutant of dynamin I^{K44A}. Internalization of transferrin receptor was blocked as expected in transfected cells expressing dynamin I^{K44A} (not shown). Enhanced levels of hWls^{wt}-HA were present at the cell surface of transfected cells expressing dynamin I^{K44A} compared with transfected cells expressing wild-type dynamin I (Fig. 1*D*). There was a significant decrease in the percentage of hWls^{wt}-HA pixels localized to the Golgi in transfected cells expressing dynamin I^{K44A} compared with transfected cells expressing wild-type dynamin I (Fig. 1*E*). Therefore, hWls is dependent on components of the clathrin-mediated pathway for internalization from the plasma membrane. Antibody-mediated internalization assays are commonly used to monitor the internalization of cell surface components. However, it was not possible to perform an internalization assay for Wls because extensive attempts to tag exofacially within the different extracellular loops of Wls were not successful as the majority of tagged Wls molecules were retained in the endoplasmic reticulum. Nonetheless, the data above clearly demonstrate that Wls accumulates at the cell surface in the absence of clathrin and dynamin.

Identification of a Tyrosine-based Motif in an Intracellular Loop of Wls—A number of well defined motifs for clathrin-mediated endocytosis have been identified (22, 23) which are found in the cytoplasmic tails of membrane proteins. However, none of these motifs is present in the 53- and 63-residue cytoplasmic tail of either human or *Drosophila* Wls. The analysis of the three intracellular loops of Wls, however, revealed a tyrosine-based Y*XXϕ* motif in the third intracellular loop of hWls. Strikingly, this YEGL sequence was conserved in mouse, rat, chicken (*Gallus gallus*), *Xenopus*, *Drosophila*, and sea urchin (*Strongylocentrotus*) (Fig. 3*A*). However, this motif was absent in the nematodes *C. elegans* and *Caenorhabditis briggsae* (Fig. 3*A*), suggesting differences in endocytosis motifs between organisms or that the YEGL sequence may be nonfunctional. To determine whether this YEGL sequence contributed to recycling of hWls, it was mutated to AEGL and the localization of hWls^{AEGL} determined in transfected HeLa cells. hWls^{AEGL}

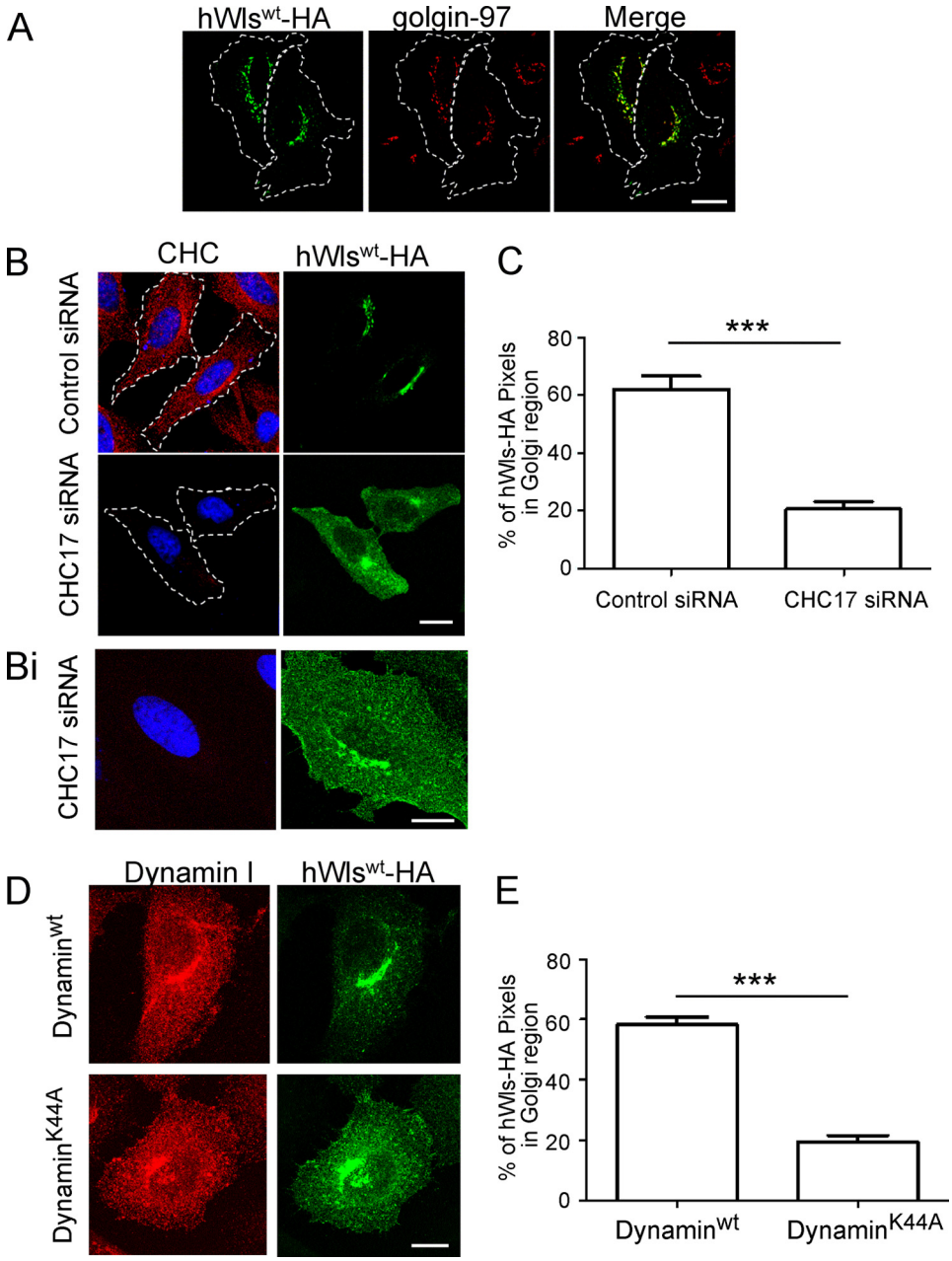

FIGURE 1. **hWls undergoes clathrin-mediated endocytosis.** *A*, HeLa cells were transfected with hWls^{wt}-HA for 24 h. Monolayers were fixed, permeabilized, and stained with monoclonal anti-HA antibodies (*green*) followed by monoclonal antibodies to golgin-97 (*red*). *B*, HeLa cells were transfected with control siRNA or CHC17 siRNA for 48 h followed by transfection with hWls^{wt}-HA for a further 24 h. Cells were fixed and permeabilized and stained with monoclonal anti-HA antibodies (*green*) and monoclonal antibodies to clathrin heavy chain (CHC) (*red*). Single optical sections were collected. *Bi*, a three-dimensional reconstruction of a single cell was made by collecting 40 optical slices at 0.40-μm intervals and converted into a *Z* stack using Leica LCS Software. *D*, HeLa cells were co-transfected with hWls^{wt}-HA and either dynamin I^{wt} or dynamin I^{K44A}. After 24 h, cells were fixed and permeabilized and stained with anti-HA antibodies (*green*) and goat polyclonal anti-dynamin I antibodies (*red*). Nuclei were stained with DAPI. *Scale bars* represent 10 μm. *C* and *E*, hWls^{wt}-HA was quantified at the Golgi of siRNA-treated cells (*C*) or dynamin I-expressing cells (*E*). Shown are the proportion of HA pixels within the Golgi region relative to the total number of HA pixel/cell, expressed as the mean ± S.E. (*error bars*) ($n = 20$ for each dataset). ***, $p < 0.001$.

showed a marked difference in localization compared with hWls^{wt}. Compared with the steady-state distribution of hWls^{wt}, hWls^{AEGL} localized predominantly to the cell surface, and much lower levels were detected in the Golgi region (Fig. 3, *B*, *Bi*, and *C*), indicating a block in internalization. In plasma lawn preparations, HA staining revealed a 30-fold higher level of HA signal in cells transfected with the hWls^{AEGL} mutant compared with the hWls^{wt} construct (see Fig. 5, *A* and *C*). The HA pixels associated with membrane lawns were quantified and normalized for the total membrane on coverslips (by Tx Red-ConA staining) and the relative expression levels of the HA construct by Western blotting (see Fig. 5, *B* and *C*). These data show that the hWls^{AEGL} mutant is retained at the cell surface.

Treatment of transfected cells with brefeldin A for either 1 h or 4 h had no apparent effect on the level of cell surface hWls^{AEGL}, indicating a long residency time at the plasma membrane (data not shown). Moreover, the distribution of hWls^{AEGL} was unaffected by silencing CHC17 (Fig. 3, *D* and *E*) and by dynamin I^{K44A} (not

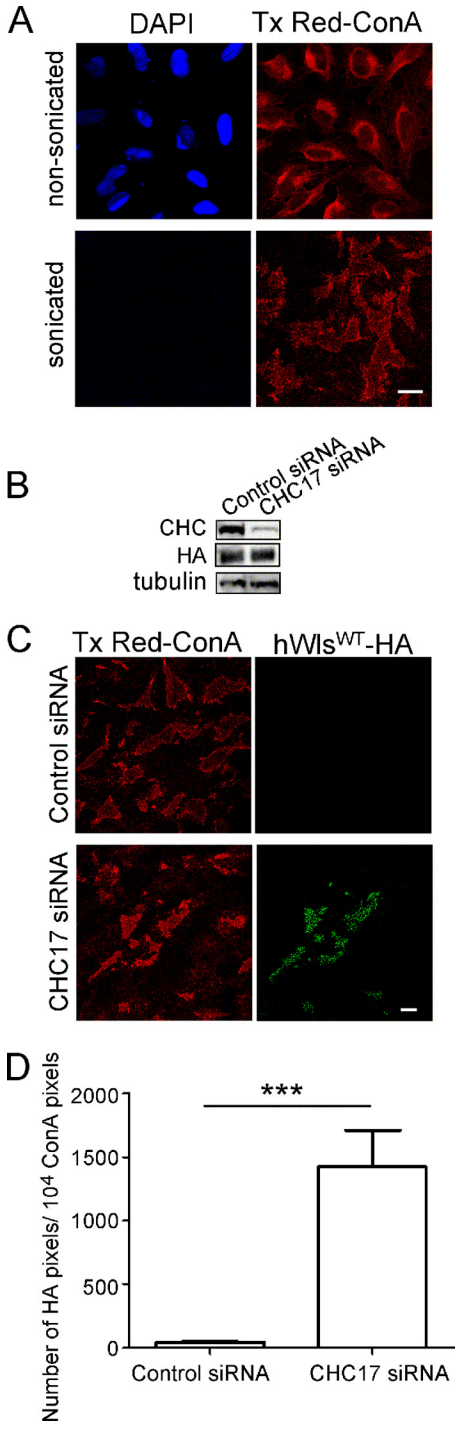

FIGURE 2. **Localization of hWls^{wt}-HA in plasma membrane lawns of CHC17-depleted cells.** *A*, HeLa cells were seeded on poly-L-lysine coverslips for 24 h and fixed or treated with swelling buffer and sonicated before fixation. Cells were permeabilized and stained with Tx Red-ConA (*red*) and DAPI (*blue*). *B–D*, HeLa cells were transfected with control siRNA or CHC17 siRNA for 48 h followed by transfection with hWls^{wt}-HA for a further 24 h. *B*, for immunoblotting, cells were lysed in SDS-PAGE reducing buffer, and cell extracts were subjected to SDS-PAGE on a 4–12% gradient polyacrylamide gel. Proteins were transferred to a PVDF membrane and probed with mouse anti-clathrin heavy chain antibodies and anti-HA antibodies using a chemiluminescence detection system. The membrane was then stripped and reprobed with mouse anti-α-tubulin antibodies. *C*, siRNA-treated cells were sonicated, fixed and blocked, and stained with Tx Red-ConA (*red*) and monoclonal anti-HA antibodies (*green*). *D*, the number of HA pixels in transfected, sonicated cells was quantified. Data are expressed as the mean number of HA pixels/10^4 Tx Red-ConA pixels ± S.E. (*error bars*) ($n = 20$ for each dataset) and normalized for densitometry values from the HA Western blot. ***, $p < 0.001$. *Scale bars* represent 10 μm.

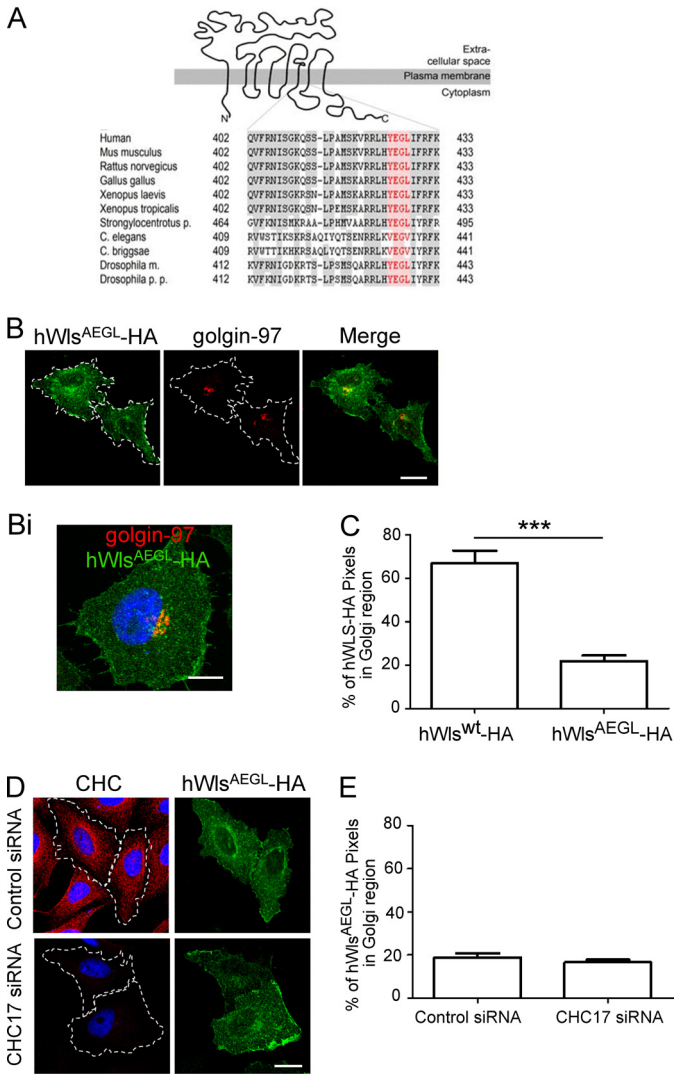

FIGURE 3. **A conserved YEGL motif in an intracellular loop of Wls is required for endocytosis.** *A*, topology of Wls (15) and alignment of the sequences of the third intracellular loop of Wls proteins are shown. Identical residues are indicated in *gray shading*, and the residues of the YEGL motif (amino acids 425–428 in human Wls) are in *red*. The following sequences of Wls were used to generate the alignment: human (ABD58927.1), *Mus musculus* (NP_080858.3), *Rattus norvegicus* (NP_955440), *Gallus gallus* (NP_001026465.1), *Xenopus laevis* (AAH89301), *Xenopus tropicalis* (NP_001016910.1), *Strongylocentrotus purpuratus* (XP_785250), *Caenorhabditis briggsae* (CAE73274), *Caenorhabditis elegans* (NP_001022275), *Drosophilia melanogaster* isoform B (NP_72961), *Drosophilia pseudoobscura pseudoobscura* (XP_001353936.2). *B*, HeLa cells were transfected with hWls^{AEGL}-HA for 24 h. Monolayers were fixed, permeabilized, and stained with monoclonal anti-HA antibodies (*green*) and monoclonal anti-golgin-97 antibodies (*red*). Single optical sections were collected. *Bi*, a three-dimensional reconstruction of a single cell was made by collecting 40 optical slices at 0.40-μm intervals and converted into a *Z* stack using Leica LCS Software. *D*, HeLa cells were transfected with control siRNA or CHC17 siRNA for 48 h followed by transfection with hWls^{AEGL}-HA for a further 24 h. Cells were fixed and permeabilized and stained with monoclonal anti-HA antibodies (*green*) and monoclonal antibodies to clathrin heavy chain (CHC) (*red*). Nuclei were stained with DAPI. *Scale bars* represent 10 μm. *C* and *E*, hWls^{wt}-HA and hWls^{AEGL}-HA were quantified at the Golgi (*C*) and hWls^{AEGL}-HA at the Golgi of siRNA-treated cells (*E*). Shown are the proportion of HA pixels within the Golgi region relative to the total number of HA pixels/cell, expressed as the mean ± S.E. (*error bars*) ($n = 20$ for each dataset). ***, $p < 0.001$.

shown). Therefore, hWls^{AEGL} showed a much higher level at the cell surface compared with hWls^{wt}, suggesting that YEGL in the third intracellular loop of human Wls sequence is a functional endocytosis motif.

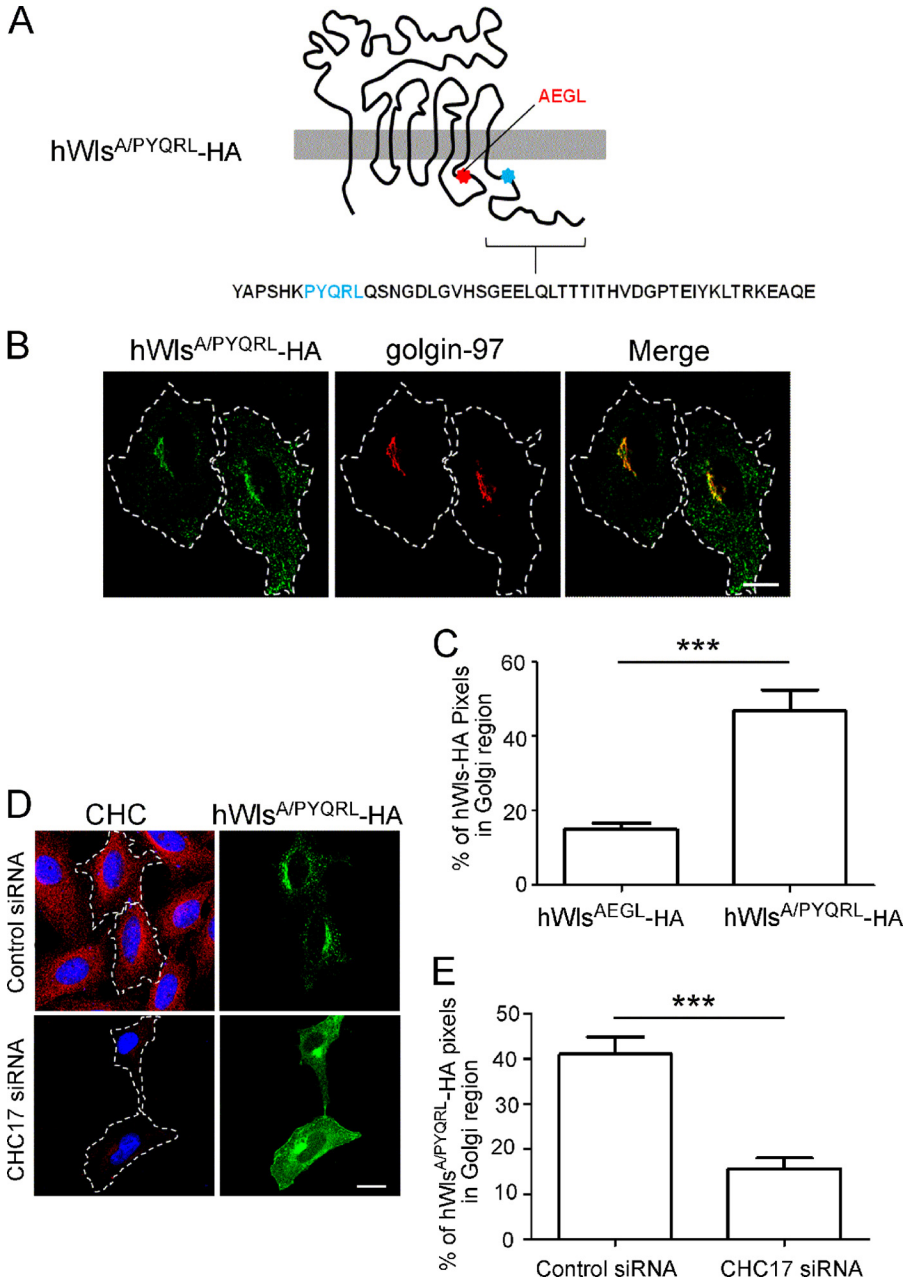

FIGURE 4. **The hWls^{AEGL}-HA mutant is rescued with a functional Y*XXϕ* motif inserted into the cytoplasmic tail.** *A*, hWls$^{A/PYQRL}$-HA construct is diagrammed. *B*, HeLa cells were transfected with hWls$^{A/PYQRL}$-HA for 24 h, and monolayers were fixed, permeabilized, and stained with monoclonal anti-HA antibodies (*green*) and monoclonal anti-golgin-97 antibodies (*red*). *D*, HeLa cells were transfected with control siRNA or CHC17 siRNA for 48 h followed by transfection with hWls$^{A/PYQRL}$-HA for a further 24 h. Cells were fixed and permeabilized and stained with monoclonal anti-HA antibodies (*green*) and monoclonal antibodies to clathrin heavy chain (*CHC*) (*red*). Nuclei were stained with DAPI. *Scale bars* represent 10 μm. *C* and *E*, hWls^{AEGL}-HA and hWls$^{A/PYQRL}$-HA were quantified at the Golgi (*C*) and hWls$^{A/PYQRL}$-HA at the Golgi of siRNA-treated cells (*E*). Shown are the proportion of HA pixels within the Golgi region relative to the total number of HA pixels/cell, expressed as the mean ± S.E. (*error bars*) ($n = 20$ for each dataset). ***, $p < 0.001$.

To confirm that the AEGL mutation caused a *bona fide* internalization defect, rather than cell surface retention due to indirect effects such as folding perturbations, we attempted to rescue the internalization defect of the hWls^{AEGL} mutant. A well defined Y*XXϕ* motif based on interaction with the μ2 subunit of the AP2 complex in yeast two-hybrid interactions (24) was selected (PYQRL) and inserted at a TM-proximal position in the cytoplasmic tail of hWls^{AEGL} (Fig. 4*A*). Expression of the hWls-AEGL/PYQRL construct (designated hWls$^{A/PYQRL}$) in HeLa cells revealed a much lower level of cell surface staining compared with the AEGL mutant. Rather, hWls$^{A/PYQRL}$ showed a predominantly Golgi localization with ~40% of the total cell hWls$^{A/PYQRL}$ located at the Golgi (Fig. 4, *B* and *C*). Analysis of plasma membrane lawns also showed a dramatically reduced level of cell surface hWls$^{A/PYQRL}$ compared with hWls^{AEGL} (Fig. 5, *A* and *C*); indeed the level of cell surface hWls$^{A/PYQRL}$ was very similar to wild-type Wls. These data confirm that the YQRL motif in the hWls$^{A/PYQRL}$ construct rescues the internalization of this mutant. CHC17 depletion of hWls$^{A/PYQRL}$-transfected cells resulted in a reduction in Golgi-localized hWls$^{A/PYQRL}$ and an increase in cell surface levels (Fig. 4, *D* and *E*). These data demonstrate

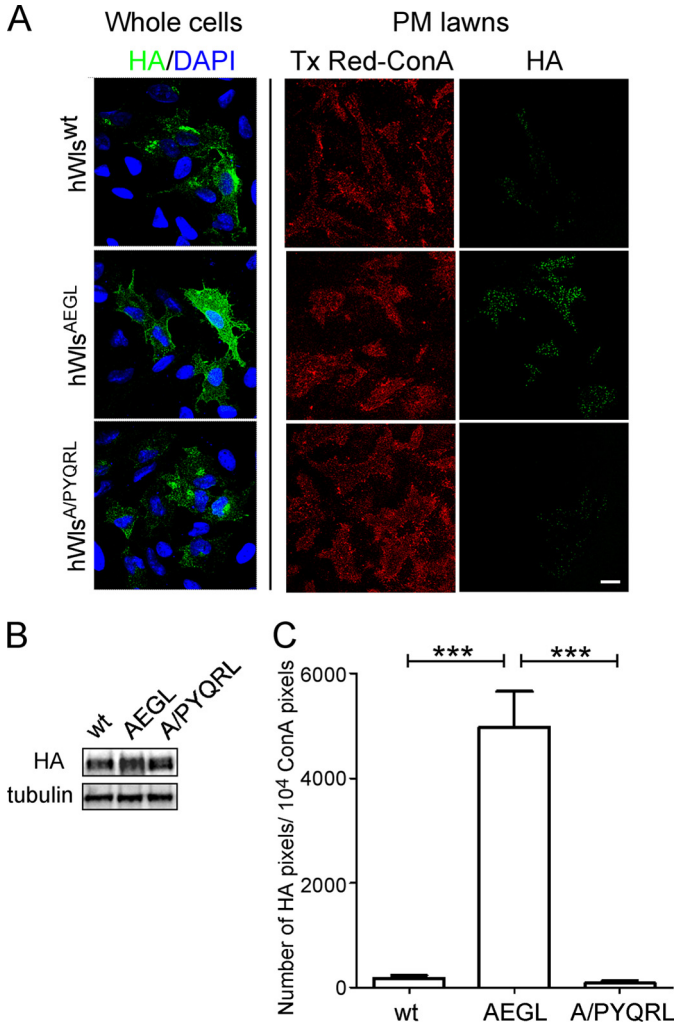

FIGURE 5. **The hWls$^{A/PYQRL}$ mutant rescues the AEGL internalization defect.** *A*, HeLa cells were seeded on poly-L-lysine coverslips and transfected with hWls^{wt}-HA, hWls^{AEGL}-HA, or hWls$^{A/PYQRL}$-HA for 24 h. Monolayers were either directly fixed and permeabilized (whole cells) and stained with monoclonal HA antibodies (*green*) and DAPI (*blue*) or treated with hypotonic buffer (*PM lawns*) followed by fixation and stained with Tx Red-ConA (*red*) and monoclonal HA antibodies (*green*). *Scale bar* represents 10 μm. *B*, immunblotting of transfected cell populations from *A*. Transfected monolayers were lysed in SDS-PAGE reducing buffer and cell extracts subjected to SDS-PAGE on a 4–12% gradient polyacrylamide gel. Proteins were transferred to a PVDF membrane and probed with rabbit anti-HA antibodies using a chemiluminescence detection system. The membrane was then stripped and reprobed with mouse anti-α-tubulin antibodies. *C*, the number of HA pixels in transfected, sonicated cells was quantified. Data are expressed as the mean number of HA pixels/10^4 Tx Red-ConA pixels, $\pm$ S.E. (*error bars*) ($n = 20$ for each dataset) and normalized for densitometry values from the HA Western blot. ***, $p < 0.001$.

that the hWls$^{A/PYQRL}$ mutant construct undergoes clathrin-mediated endocytosis, thereby demonstrating that the internalization block of the AEGL mutation was likely due to the inability to recruit endocytic machinery directly.

Drosophila Wls^{AEGL} Mutant Displays a Wing Notch Phenotype—To determine the functional consequences of specifically inhibiting the recycling of Wls, transgenic *Drosophila* Wls^{AEGL} (dWls^{AEGL}) flies were generated on a *wls*-null background. The *wls*^{1} allele is lethal, and the dWls^{AEGL} transgene rescued approximately 50% of the expected number of flies compared with the wt transgene. Of these recued flies, 100% showed a wing phenotype and a reduced number of bristles at the anterior wing margin (Fig. 6, *A*–*C*). This phenotype is typical for reduced/loss of Wnt signaling. In contrast, flies with a Wls^{wt} transgene on a *wls*^{1} background showed no phenotype. The wings in the rescued flies appear a little smaller compared with the wt control flies (*yw* control) (Fig. 6, *A*–*C*). However, there was no observed difference in wing size between transgenic dWls^{wt} and dWls^{AEGL} flies. The localization of Wls was examined in the *Drosophila* wing imaginal disc. Wls was expressed ubiquitously in the wing discs of dWls^{wt} and dWls^{AEGL} transgenics. As expected, wt dWls was observed at high levels in a stripe of cells at the dorsal-ventral boundary (the *wg* expression domain). Notably, the relocalization of dWls^{AEGL} appears to be disturbed because the enhanced signal for Wls observed in the cells expressing *wg* is lost compared with the wt Wls transgene. The dorsal-ventral boundary cells express high levels of Wg (Fig. 6*E*), and Wg is found in small punctate structures that decrease in number with increasing distance from the Wg source. These punctate Wg-positive structures are secreted Wg protein (25). Notably, there are fewer Wg-positive punctate structures in the dWls^{AEGL} mutant compared with dWls^{wt} (see Fig. 6, *E* and *H*, *insets*), indicating reduced levels of secreted Wg.

Hence, the dWls^{AEGL} mutation appears to affect the recycling of Wls in Wg-secreting cells resulting in reduced Wg secretion. To analyze for altered Wg secretion directly, the expression of the Wg target gene, *sens*, was examined. There was a considerable reduction in levels of *sens* in the wing discs of the dWls^{AEGL} transgenic compared with dWls^{wt} (Fig. 6, *F* and *I*), demonstrating a reduced level of Wnt signaling. Collectively, these results show that the YEGL motif of dWls is required for the plasma membrane-Golgi recycling of dWls, a trafficking route that is necessary for efficient Wnt secretion and signaling.

DISCUSSION

The internalization and intracellular trafficking of the sorting receptor Wls are required for the secretion of Wnt signaling proteins (15, 16). To date, the importance of Wls recycling has been examined by the silencing and knockout of components of the trafficking machinery, whereas the signals/motifs for internalization and endosomal sorting of Wls had not been identified. Here, we sought to identify the internalization motif of Wls to allow the generation of Wls mutants that are blocked in recycling of this specific cargo. Our study has revealed a tyrosine-based endocytosis motif in the third extracellular loop of Wls that is necessary for internalization of the protein. Mutation of the essential tyrosine in the YEGL motif resulted in cell surface retention of Wls and a Wnt signaling phenotype in transgenic flies. The rescue of the hWls^{AEGL} mutation by insertion of a classical $YXX\phi$ motif in the cytoplasmic tail of hWls^{AEGL} supports the conclusion that the cell surface retention of hWls^{AEGL} is due to the loss of a functional endocytosis motif. Collectively, the data presented in this paper identify an endocytosis motif in an unusual location in the protein sequence and provide direct evidence that the endocytosis and recycling of Wls are required for efficient secretion of Wnt signaling proteins.

Motifs for clathrin-mediated endocytosis are typically found in the cytoplasmic tails of membrane proteins (22), and to our knowledge this is the first report of a $YXX\phi$ endocytosis motif within an intracellular loop of a multipass membrane protein.

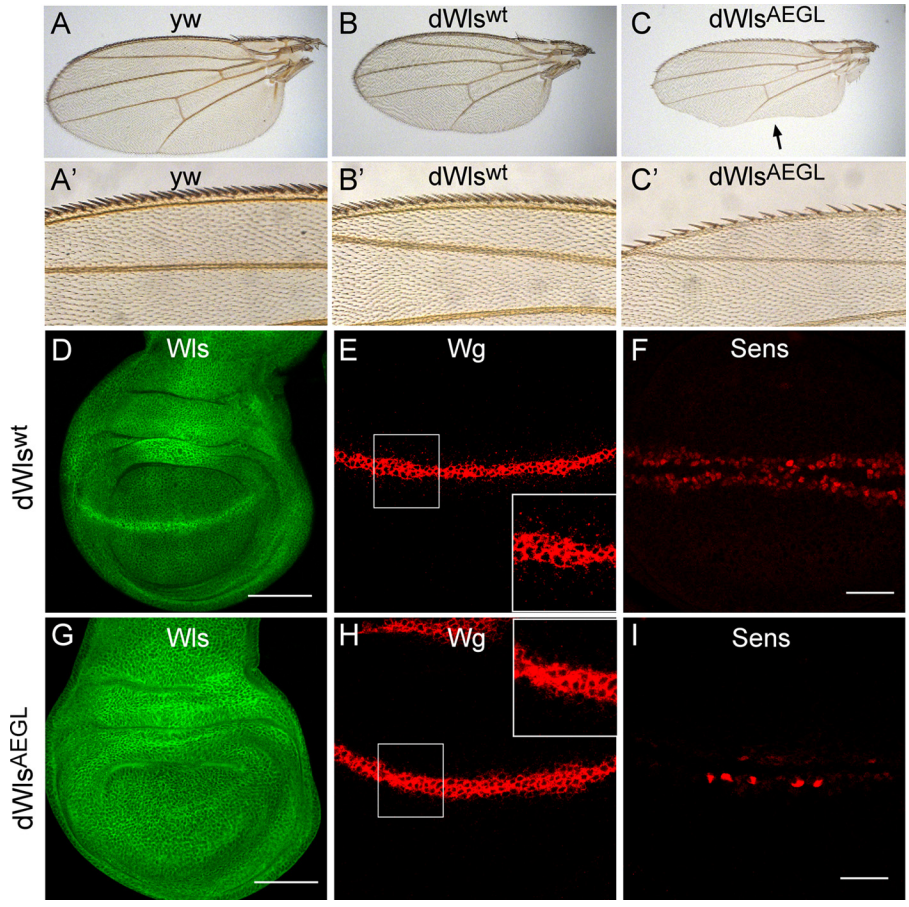

FIGURE 6. **YEGL motif of *Drosophila* Wls is required for Wg secretion and signaling.** *A–C*, adult wings are oriented proximal to the *right*, anterior up. Adult wings of control (*A*), dWls^{wt} transgene (*B*), and dWls^{AEGL} mutant (*C*) are shown. The wings of flies rescued with dWls^{AEGL} transgene have notches at the posterior margin (*arrow*). *A′–C′* magnification of the anterior wing bristles. Fewer Wg-dependent bristles are present in the dWls^{AEGL} (*C′*). *D–I*, wing imaginal discs were stained for Wls (*D* and *G*), Wg (*E* and *H*), and Sens (*F* and *I*). In *D* and *G*, Wls transgenes are ubiquitously expressed in wing imaginal disc. Note the prominent stripe of enhanced Wls staining in the dorsal-ventral boundary in the dWls^{wt} which is absent in the dWls^{AEGL} mutant. In *E* and *H*, a Wg gradient and Wls^{wt} transgene discs show a substantial amount of Wg antigen in punctate structures. This gradient is less prominent in the dWls^{AEGL} mutant. *Insets* are a high magnification of boxed regions. In *F* and *I*, note that the Wg target gene *sens* is much less induced in the dWls^{AEGL} mutant (*I*) compared with the wt transgene (*F*).

Endocytosis motifs in intracellular loops could have relevance to other multipass membrane proteins that undergo endocytosis, such as ion channels and G protein-coupled receptors (26, 27). Whereas cytoplasmic tails can be readily inserted into chimeric reporter proteins for detailed analysis of endocytosis motifs (23), analyses of intracellular loops in isolation of the remainder of the membrane protein are more problematic because the structures of the intracellular loops are likely to be dependent on the correct membrane topology.

Under steady-state conditions the majority of wild-type hWls is located at the Golgi, whereas in CHC17-depleted cells hWls accumulates predominantly at the cell surface, indicating that the bulk of the protein is recycling via the plasma membrane. Wls^{AEGL} accumulates at the cell surface and also mimics the steady-state distribution of wild-type Wls in CHC17-depleted cells, indicating that the Y425A mutation of Wls^{AEGL} is inhibiting endocytosis. The insertion of a classical endocytosis motif in the cytoplasmic tail of Wls^{AEGL} reduced the cell surface level of the construct to that observed for wild-type Wls, demonstrating that the accumulation of Wls^{AEGL} at the cell surface was not due to aberrant folding but rather the loss of an endocytosis motif.

Internalization of Wls is dependent on clathrin, dynamin (this work), and also AP2 (10, 11). Given that the YEGL sequence in the third intracellular loop of hWls is required for internalization and that AP2 is the main clathrin adaptor at the cell surface, it is highly likely that this tyrosine-based sequence is a functional AP2 motif. Attempts to show a direct interaction of Wls with AP2 *in vivo* by immunoprecipitation were not successful. However, it should be noted that AP2 interactions with cargo are dynamic and transient (28), and there are only a few cases where AP2 interactions with cargo been demonstrated *in vivo* (29–31). Notably, a YEGL motif has been identified as an internalization signal in other proteins, for example Igα (human) (24), thus this Y motif *per se* is known to be a function signal. The selective recruitment of AP2 to the plasma membrane requires an interaction not only with the *YXXϕ* motif but also with phosphoinositide 4,5-bisphosphate, which is enriched at the plasma membrane (32). Interestingly, the rescue of the hWls^{AEGL} phenotype was successful when a classical *YXXϕ* motif was inserted in the cytoplasmic tail close to the transmembrane domain, whereas the insertion of the motif at the C terminus of the cytoplasmic tail did not rescue endocytosis of hWls^{AEGL}.[5] A recent study by Owen and co-workers (33) has

[5] P. Z. C. Chia and P. A. Gleeson, unpublished data.

uncovered the mechanism for the high affinity interaction of AP2 with cargo proteins at the plasma membrane. The binding of the AP2 complex to phosphoinositide 4,5-bisphosphate results in a conformational change of AP2 to the open configuration, which can then interact with the *YXXϕ* motif on endocytic cargo. It is therefore likely that the *YXXϕ* motif has to be in close proximity to the phosphoinositide 4,5-bisphosphate-rich lipid bilayer to facilitate the simultaneous interaction of AP2 with both the cargo and the cytoplasmic leaflet of the lipid bilayer. Indeed, the importance of the distance of internalization motifs in the cytoplasmic tail in relation to the lipid bilayer has been highlighted previously (22).

We demonstrated that the Y425A mutation of Wls resulted in a *bona fide* endocytosis defect by the ability to rescue the phenotype with a functional *YXXϕ* motif inserted in its cytoplasmic tail. The insertion of the *YXXϕ* resulted in the rescue of the internalization of Wls^{AEGL} with 40% located within the Golgi region under steady-state conditions. One question that arises is whether the YEGL motif is used only as an endocytosis signal or used for both endocytosis and for retromer- and/or AP1-mediated endosome-to-Golgi retrograde transport. If the former is the case then one may expect that $hWls^{A/PYQRL}$ would be internalized and trafficked to lysosomes. The steady-state distribution of $hWls^{A/PYQRL}$ showed a high level of Golgi enrichment that may suggest that the YEGL motif is an endocytosis signal distinct from signal(s) required for retrograde endosome-to-TGN transport. However, there are caveats to this interpretation. Tyrosine-based motifs are recognized not only at the plasma membrane but also at several intracellular sorting locations, and the factors that contribute to the differential sorting of *YXXϕ* motifs at the various locations are not well understood. One factor relevant to the sorting of plasma membrane proteins to the lysosome is the spacing of the tyrosine-based motif relative to the membrane (34). Although the spacing of the PYQRL motif in the cytoplasmic tail of $hWls^{A/PYQRL}$ is consistent with sorting to the lysosome, it is difficult to predict with certainty the intracellular trafficking defined by the PYQRL motif and therefore the contribution of this motif to the intracellular localization of $hWls^{A/PYQRL}$.

The YEGL motif of Wls is conserved in human, mouse, rat, chicken, *Xenopus*, *Drosophila*, and sea urchin but is absent in worms. As for *Drosophila*, *Xenopus*, and humans, the trafficking of Wls from *C. elegans* has been proposed to be regulated by the AP2 adaptor and by retromer (10). Hence, the *C. elegans* Wls would also be expected to have a motif for clathrin-mediated endocytosis. There has been considerable debate regarding the evolutionary relationship of nematodes with arthropods and chordates (35, 36). A traditional view is that nematodes represent an outgroup of the animals with a true body cavity (coelomates) (35). Given the current debate on the phylogenics of these species, it is perhaps not surprising to find a conserved sequence in coelomata, but missing in *C. elegans*. Interestingly, there is *YXXϕ* motif (YNRI) in Wls of both *C. elegans* and *C. briggsae* at position 260–263 within the second intracellular loop, a motif that is absent from the other species listed in Fig. 1. Thus, this alternative Y-based motif may function as an endocytosis signal in worms. Another possibility is the presence of a cluster of serine and threonine residues in the third intracellular loop of *C. elegans* and *C. briggsae* which could represent a potential phosphorylation motif for binding by the adaptor protein, β-arrestin. β-Arrestin interacts with elements of the endocytic machinery such as AP2 and clathrin and promotes endocytosis, a mechanism employed by agonist-dependent internalization of G protein-coupled receptor (37). Regardless, the identification of endocytosis motifs of human and *Drosophila* Wls has allowed the relevance of the trafficking of this cargo receptor to be specifically assessed in complex organisms within the context of normal trafficking machinery.

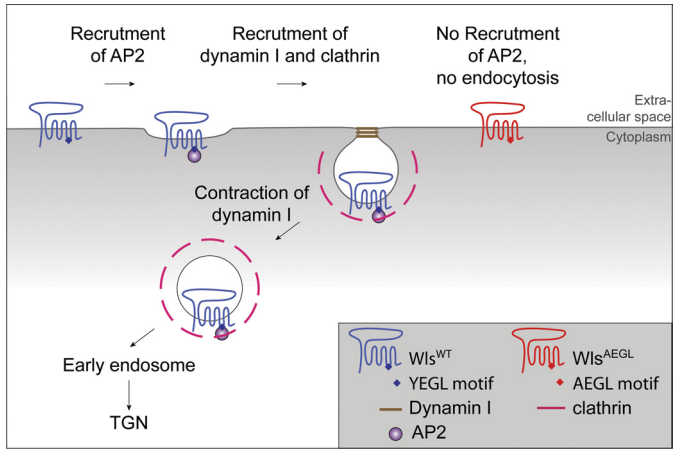

FIGURE 7. **Model for the internalization and recycling of Wls.** Newly synthesized Wls is transported by the anterograde transport pathway from the TGN to the cell surface. At the cell surface Wls is recruited into clathrin-coated pits by interaction of the adaptor AP2 with the YEGL motif in the third intracellular loop of Wls. Internalization of Wls by clathrin-mediated endocytosis requires dynamin I. Internalized Wls is then recycled to the TGN by retrograde transport from the early endosomes. Mutation of the YEGL motif in the third intracellular loop of Wls results in an internalization-defective Wls which accumulates on the cell surface and is blocked in recycling.

A proposed model for the recycling of Wls is shown in Fig. 7. Newly synthesized Wls is transported to the cell surface and, based on previous studies (16), is proposed to escort Wnt proteins from the TGN to the cell surface. From the cell surface the recycling of Wls back to the TGN is dependent on clathrin-AP2-mediated endocytosis for transport to early endosomes and then retromer-dependent transport from early endosomes to the TGN. In the absence of the tyrosine endocytosis motif, Wls accumulates on the cell surface and is recycled inefficiently to the TGN. This results in a protein that cannot be recycled for further rounds of Wnt secretion and is effectively a one-use receptor. Importantly, the propensity of the AEGL transgene to rescue *wls*-null flies demonstrates that the AEGL mutant is functional as a cargo receptor to chaperone Wnt transport from the TGN to the cell surface for secretion. The finding that $dWls^{AEGL}$ flies have a reduced Wnt signaling phenotype is consistent with the proposal that Wls^{AEGL} can only facilitate Wnt secretion once during its lifetime due to the block in endocytosis. Thus, through this study, we have directly shown that efficient trafficking of the Wls protein is required for normal Wnt signaling.

Acknowledgments—We thank F. Port, G. Hausmann, and S. Ralph for discussions.

REFERENCES

1. Logan, C. Y., and Nusse, R. (2004) *Annu. Rev. Cell Dev. Biol.* **20,** 781–810
2. Bänziger, C., Soldini, D., Schütt, C., Zipperlen, P., Hausmann, G., and Basler, K. (2006) *Cell* **125,** 509–522
3. Bartscherer, K., Pelte, N., Ingelfinger, D., and Boutros, M. (2006) *Cell* **125,** 523–533
4. Goodman, R. M., Thombre, S., Firtina, Z., Gray, D., Betts, D., Roebuck, J., Spana, E. P., and Selva, E. M. (2006) *Development* **133,** 4901–4911
5. Port, F., and Basler, K. (2010) *Traffic* **11,** 1265–1271
6. Fu, J., Jiang, M., Mirando, A. J., Yu, H. M., and Hsu, W. (2009) *Proc. Natl. Acad. Sci. U.S.A.* **106,** 18598–18603
7. Kim, H., Cheong, S. M., Ryu, J., Jung, H. J., Jho, E. H., and Han, J. K. (2009) *Mol. Cell. Biol.* **29,** 2118–2128
8. Carpenter, A. C., Rao, S., Wells, J. M., Campbell, K., and Lang, R. A. (2010) *Genesis* **48,** 554–558
9. Franch-Marro, X., Wendler, F., Guidato, S., Griffith, J., Baena-Lopez, A., Itasaki, N., Maurice, M. M., and Vincent, J. P. (2008) *Nat. Cell Biol.* **10,** 170–177
10. Pan, C. L., Baum, P. D., Gu, M., Jorgensen, E. M., Clark, S. G., and Garriga, G. (2008) *Dev. Cell* **14,** 132–139
11. Port, F., Kuster, M., Herr, P., Furger, E., Bänziger, C., Hausmann, G., and Basler, K. (2008) *Nat. Cell Biol.* **10,** 178–185
12. Yang, P. T., Lorenowicz, M. J., Silhankova, M., Coudreuse, D. Y., Betist, M. C., and Korswagen, H. C. (2008) *Dev. Cell* **14,** 140–147
13. Belenkaya, T. Y., Wu, Y., Tang, X., Zhou, B., Cheng, L., Sharma, Y. V., Yan, D., Selva, E. M., and Lin, X. (2008) *Dev. Cell* **14,** 120–131
14. Harterink, M., Port, F., Lorenowicz, M. J., McGough, I. J., Silhankova, M., Betist, M. C., van Weering, J. R., van Heesbeen, R. G., Middelkoop, T. C., Basler, K., Cullen, P. J., and Korswagen, H. C. (2011) *Nat. Cell Biol.* **13,** 914–923
15. Bartscherer, K., and Boutros, M. (2008) *EMBO Rep.* **9,** 977–982
16. Hausmann, G., Bänziger, C., and Basler, K. (2007) *Nat. Rev. Mol. Cell Biol.* **8,** 331–336
17. van der Bliek, A. M., Redelmeier, T. E., Damke, H., Tisdale, E. J., Meyerowitz, E. M., and Schmid, S. L. (1993) *J. Cell Biol.* **122,** 553–563
18. Nolo, R., Abbott, L. A., and Bellen, H. J. (2000) *Cell* **102,** 349–362
19. Huang, F., Khvorova, A., Marshall, W., and Sorkin, A. (2004) *J. Biol. Chem.* **279,** 16657–16661
20. Heuser, J. (1989) *J. Cell Biol.* **108,** 401–411
21. Petris, M. J., Mercer, J. F., Culvenor, J. G., Lockhart, P., Gleeson, P. A., and Camakaris, J. (1996) *EMBO J.* **15,** 6084–6095
22. Bonifacino, J. S., and Traub, L. M. (2003) *Annu. Rev. Biochem.* **72,** 395–447
23. Kozik, P., Francis, R. W., Seaman, M. N., and Robinson, M. S. (2010) *Traffic* **11,** 843–855
24. Ohno, H., Aguilar, R. C., Yeh, D., Taura, D., Saito, T., and Bonifacino, J. S. (1998) *J. Biol. Chem.* **273,** 25915–25921
25. Strigini, M., and Cohen, S. M. (2000) *Curr. Biol.* **10,** 293–300
26. Ferguson, S. S. (2001) *Pharmacol. Rev.* **53,** 1–24
27. Seebohm, G., Strutz-Seebohm, N., Birkin, R., Dell, G., Bucci, C., Spinosa, M. R., Baltaev, R., Mack, A. F., Korniychuk, G., Choudhury, A., Marks, D., Pagano, R. E., Attali, B., Pfeufer, A., Kass, R. S., Sanguinetti, M. C., Tavare, J. M., and Lang, F. (2007) *Circ. Res.* **100,** 686–692
28. Owen, D. J., Collins, B. M., and Evans, P. R. (2004) *Annu. Rev. Cell Dev. Biol.* **20,** 153–191
29. Collawn, J. F., Stangel, M., Kuhn, L. A., Esekogwu, V., Jing, S. Q., Trowbridge, I. S., and Tainer, J. A. (1990) *Cell* **63,** 1061–1072
30. Sorkin, A., Mazzotti, M., Sorkina, T., Scotto, L., and Beguinot, L. (1996) *J. Biol. Chem.* **271,** 13377–13384
31. Weixel, K. M., and Bradbury, N. A. (2001) *J. Biol. Chem.* **276,** 46251–46259
32. Höning, S., Ricotta, D., Krauss, M., Späte, K., Spolaore, B., Motley, A., Robinson, M., Robinson, C., Haucke, V., and Owen, D. J. (2005) *Mol. Cell* **18,** 519–531
33. Jackson, L. P., Kelly, B. T., McCoy, A. J., Gaffry, T., James, L. C., Collins, B. M., Höning, S., Evans, P. R., and Owen, D. J. (2010) *Cell* **141,** 1220–1229
34. Rohrer, J., Schweizer, A., Russell, D., and Kornfeld, S. (1996) *J. Cell Biol.* **132,** 565–576
35. Wolf, Y. I., Rogozin, I. B., and Koonin, E. V. (2004) *Genome Res.* **14,** 29–36
36. Dunn, C. W., Hejnol, A., Matus, D. Q., Pang, K., Browne, W. E., Smith, S. A., Seaver, E., Rouse, G. W., Obst, M., Edgecombe, G. D., Sørensen, M. V., Haddock, S. H., Schmidt-Rhaesa, A., Okusu, A., Kristensen, R. M., Wheeler, W. C., Martindale, M. Q., and Giribet, G. (2008) *Nature* **452,** 745–749
37. Kirchhausen, T. (1999) *Annu. Rev. Cell Dev. Biol.* **15,** 705–732
38. Lieu, Z. Z., Derby, M. C., Teasdale, R. D., Hart, C., Gunn, P., and Gleeson, P. A. (2007) *Mol. Bio. Cell* **18,** 4979–4991